Journal of Environmental Chemical Engineering 10 (2022) 107408

Contents lists available at ScienceDirect

Journal of Environmental Chemical Engineering

journal homepage: www.elsevier.com/locate/jece

Investigation of biochar from *Cedrella fissilis* applied to the adsorption of atrazine herbicide from an aqueous medium

Paola T. Hernandes [a,b], Dison S.P. Franco [c], Jordana Georgin [c], Nina P.G. Salau [b], Guilherme L. Dotto [a,b,*]

[a] Research Group on Adsorptive and Catalytic Process Engineering (ENGEPAC), Federal University of Santa Maria, Av. Roraima, 1000-7, 97105-900 Santa Maria, RS, Brazil
[b] Chemical Engineering Department, Federal University of Santa Maria, UFSM, 97105-900 Santa Maria, Brazil
[c] Department of Civil and Environmental, Universidad de la Costa, CUC, Barranquilla, Atlántico, Colombia

ARTICLE INFO

Editor: Xianwei Liu

Keywords:
Adsorption
Atrazine
Biochar
Pesticides
River water

ABSTRACT

Biochar was produced from the sawdust of the wood forest species *Cedrella fissilis* and later used as an adsorbent to remove atrazine herbicide from aqueous media. Biochar showed high thermal stability, an amorphous structure, and a highly irregular surface, mainly composed of carbon-containing bonds. The isothermal curves confirmed that the increase in temperature favored the adsorption of the herbicide. The Langmuir model best suited the experimental equilibrium data, with the maximum adsorption capacity of 7.68 mg g^{-1} at 328 K. The thermodynamic parameters confirmed a spontaneous process of an endothermic nature governed by physical interactions (interactions of van der Waals and hydrogen bonds). Kinetic studies showed that equilibrium was reached within 180 min. The linear driving force model (LDF) showed good statistical adjustment to the experimental data, where it was observed that the diffusion coefficient increased with the concentration of adsorbate. Biochar can be reused in up to three cycles. Finally, the adsorbent showed good efficiency in real water samples from rivers contaminated with atrazine, with 76.58% and 71.29% removal.

1. Introduction

Herbicides and pesticides have become increasingly common and necessary in agricultural activities in recent years to control agricultural pests, increase efficiency, and avoid economic damage. Atrazine ($C_8H_{14}ClN_5$) is one of the most widely used chlorine herbicides in agriculture [1,2]. It is a selective herbicide with high efficiency for controlling various broadleaf weeds and grasses, and it is used on a variety of crops, including corn and sugarcane. Because of its harmful effects on health, atrazine has been banned in several European countries since 1991, and the European Union as a whole banned its use in 2004. However, due to the molecule's properties, such as low biodegradability and high persistence, atrazine can still be detected in drinking water samples and even pregnant women's urine [3]. Furthermore, atrazine is still widely used in several developing countries, including China, Brazil, and Iran [4]. Extensive use in agriculture pollutes soil and water, reducing ecosystem function and posing health risks. Serious damage to human organisms includes changes in protein expression, changes at the cellular level, DNA damage, sperm mutagenesis, and disruption of endocrine hormones [2]. In terms of animals, one study found that exposure to certain levels disrupts the sexual evolution of amphibian species in the wild and reduces the overall number of animal species [1]. In addition, the herbicide inhibits photosynthetic activity and, as a result, the development and growth of aquatic plant species in aquatic systems [5,6].

Because of the serious problems caused by atrazine, the scientific community has been working to improve techniques for removing it from the environment in recent years. However, some processes are not flexible, have high costs, are inefficient, and may produce secondary contaminants [7]. Because of its low cost, ease of operation, and high efficiency, adsorption has proven to be a promising alternative [8,9]. The application of transformed biodegradable material onto usable adsorbents such as activated carbon and biochar is a key point in the adsorption process [10]. Biochar can be an effective adsorbent in removing several pollutants due to its highly porous structure, similar to activated carbon [11]. In addition, because activated carbons require

* Corresponding author at: Research Group on Adsorptive and Catalytic Process Engineering (ENGEPAC), Federal University of Santa Maria, Av. Roraima, 1000-7, 97105-900 Santa Maria, RS, Brazil.
E-mail address: guilherme.dotto@ufsm.br (G.L. Dotto).

https://doi.org/10.1016/j.jece.2022.107408
Received 17 December 2021; Received in revised form 1 February 2022; Accepted 12 February 2022
Available online 16 February 2022

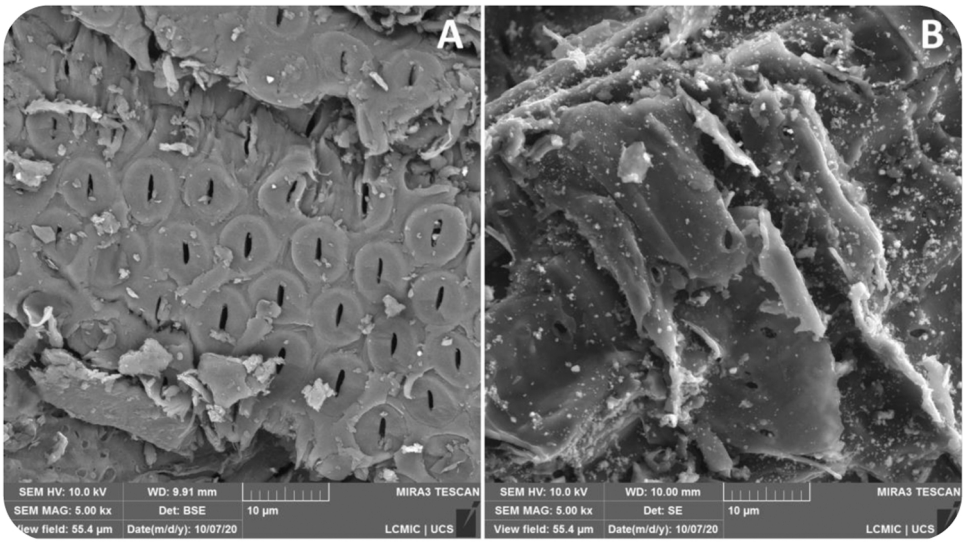

Fig. 1. SEM images for CBS (A) and BCC (B) (x5000).

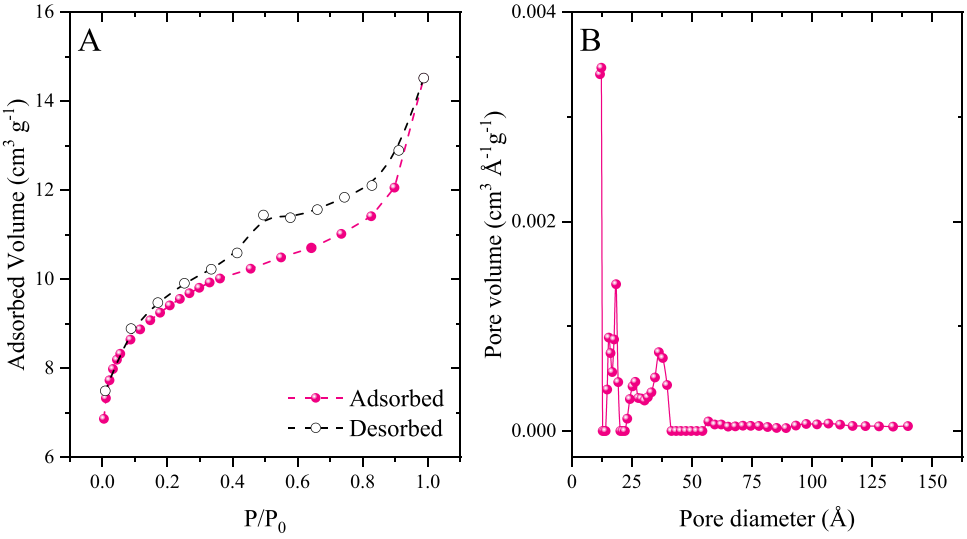

Fig. 2. N_2 adsorption-desorption isotherms (a) and desorption pore size distribution (b) for the BCC.

Table 1
Amounts of C and O in the biochar.

Element % by weight	CBS	BCC
C (%)	65.65	88.40
O (%)	33.04	10.61
O/C	0.503	0.120

Table 2
Functional groups of CBS and BCC.

Functional Group	Wavenumber (cm^{-1})	
	CBS	BCC
O-H	3444	3444
C-H	2922	–
C═C	1650	–
C═C	1510	1510
C-O	1052	–

reagents in their activation process, whereas biochars do not, the latter have a lower preparation cost and produce fewer effluents [12].

In recent years, several carbonaceous compounds have been successfully used to remove herbicides [13–17,20–24]. The species *Cedrella fissilis* is used in the wood industry. It presents a wood with high resistance, high growth rates, and good adaptability to edaphic conditions, mainly Minas Gerais and Bahia (Brazil). Due to these factors, commercial plantations have grown, and consequently, the volume of residual biomass in their processing, such as bark and sawdust, has also increased [25]. The bark corresponds to residues generated in the primary splitting of the wood, generally being deposited in the plantation field itself. In contrast, the sawdust corresponds to the waste generated by the secondary splitting and is generated in large volumes in the sawmills. In adsorption studies, the residual bark of the *Cedrella fissilis* was used to remove red 97 from the aqueous solution [25]. However, no reports of the use of *C. fissilis* biochar in the removal of atrazine have been published to date.

The current study used sawdust from *Cedrella fissilis* as the raw material for biochar production. Biochar was produced at temperatures of up to 800 °C. Fourier transform infrared spectroscopy (FTIR), X-ray diffraction (DRX), scanning electron microscopy (SEM),

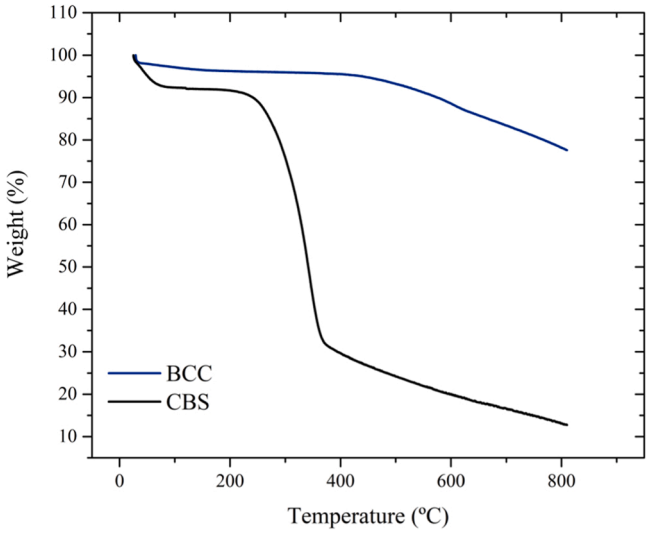

Fig. 3. TGA curves of CBS and BCC.

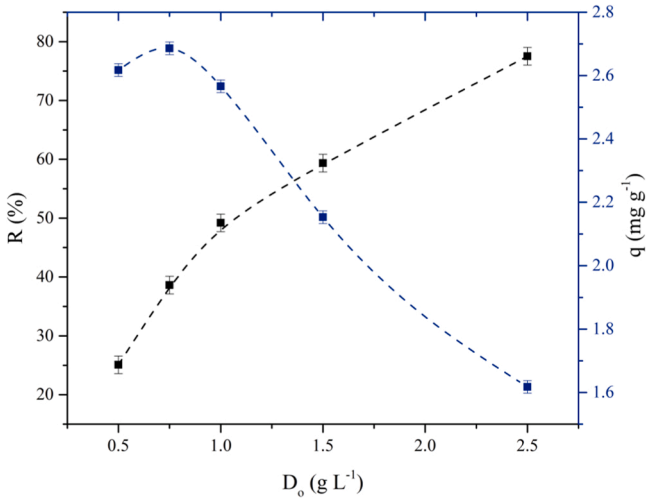

Fig. 4. Effect of BCC dosage on atrazine adsorption.

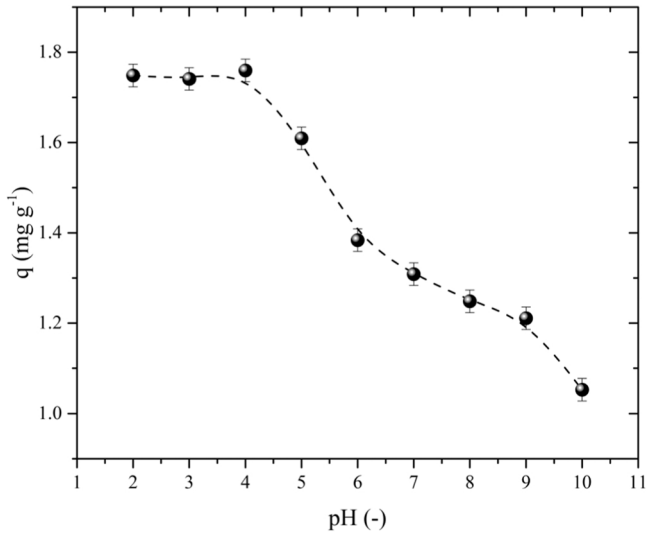

Fig. 5. Effect of pH on atrazine adsorption.

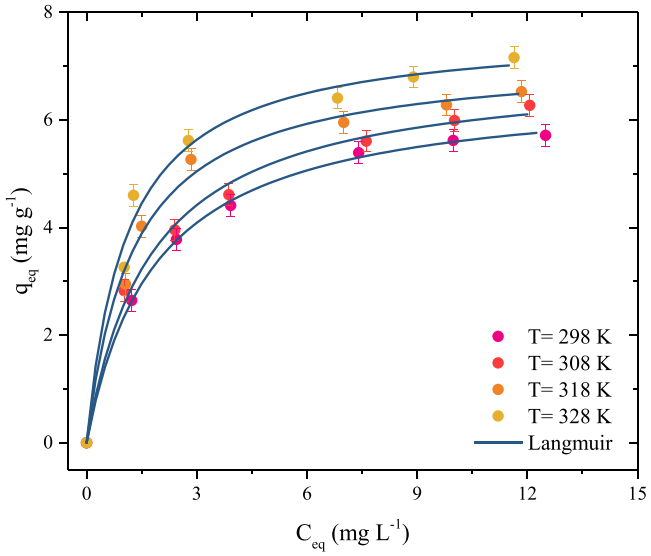

Fig. 6. Adsorption isotherms for the atrazine onto the BCC.

thermogravimetric analysis (TGA), and Brunner, Emmet, and Teller (BET) methods were used to examine the properties of the original and carbonized materials. The biochar's ability to absorb atrazine herbicide was then tested. First, dosage and pH analysis were predetermined, followed by isothermal studies and thermodynamic parameter analysis. Next, kinetic studies were investigated and fitted to the linear driving force model (LDF). Following that, studies on adsorbent regeneration were conducted. Finally, the material's performance against a mixture of river water containing atrazine was evaluated.

2. Materials and methods

2.1. Reactants employed

For this study, the following compounds were used: hydrochloric acid (HCl), sodium hydroxide (NaOH), and atrazine (chemical formula: $C_8H_{14}ClN_5$, M_w: 215.7 g mol^{-1}, molar volume: 169.8 cm^{-3} mol^{-1}). All chemicals were acquired with an analytical grade from Sigma-Aldrich. Atrazine stock solutions were previously prepared by dissolving 50 mg L^{-1} of atrazine in water. Deionized water was employed in the stock solution preparation and all subsequent dilutions.

2.2. Biochar preparation and characterization

Cedrella fissilis sawdust was obtained from a wood industry in the Brazilian state of Rio Grande do Sul. Approximately 600 g of sawdust was oven-dried for 4 h at 333 K. The material was sieved, yielding a fraction with particles smaller than 1 mm in size. The precursor fraction was called CBS, and a portion of it was separated for characterization analysis, while the remainder was used to produce biochar.

Pyrolysis was performed in a quartz tube under an N_2 atmosphere at a flow rate of 0.25 L min^{-1} and a heating rate of 10 °C min^{-1} until the temperature reached 800 °C. When the temperature reached its maximum, the precursor material was kept for 60 min before cooling and maintained for 12 h at 353 K. Finally, the biochar was labeled BBC, with a small portion separated for characterization and the remainder used in atrazine adsorption experiments. The characterization methodology and equipment employed are described in Supplementary Material S1.

2.3. BBC and atrazine batch experiments

A thermostatic shaker (MA093, Marconi, Brazil) conducted atrazine

Table 3
Isotherm parameters for the atrazine and BCC system.

Model	Temperature (K)			
	298	308	318	328
Langmuir				
q_L(mg g^{-1})	6.6403	6.9961	7.1867	7.6791
K_L (L mg^{-1})	0.53427	0.57105	0.78507	0.91721
R^2	0.99920	0.99510	0.99281	0.98706
R^2_{adj}	0.99880	0.99265	0.98921	0.98058
ARE (%)	1.0217	3.3252	3.9907	5.2837
MSR (mg g^{-1})^2	4.0808×10^{-3}	2.8646×10^{-2}	4.7230×10^{-2}	9.9019×10^{-2}
Freundlich				
K_F ((mg g^{-1})(mg L^{-1})$^{-1/nF}$)	2.8006	2.9695	3.5193	3.9735
$1/n_F$(dimensionless)	0.3013	0.3062	0.2608	0.2479
R^2	0.98792	0.99788	0.97333	0.97506
R^2_{adj}	0.98188	0.99682	0.95999	0.96259
ARE (%)	4.9819	2.2524	7.0803	7.0322
MSR (mg g^{-1})^2	6.1655×10^{-2}	1.2406×10^{-2}	1.7519×10^{-1}	1.9076×10^{-1}
Dubinin-Radushkevich				
q_{mDR} (mol kg)$^{-1}$	0.52530	0.59147	0.40123	0.38685
β (mol J)^2	0.12166	0.11962	0.09867	0.09094
R^2	0.98792	0.99788	0.97333	0.97506
R^2_{adj}	0.98551	0.99745	0.96799	0.97008
ARE (%)	4.2745	1.9304	6.0687	6.0260
MSR (mg g^{-1})^2	5.7600×10^{-4}	6.5200×10^{-4}	7.2800×10^{-4}	8.6400×10^{-4}
q_{exp} (mg g^{-1})	5.7153	6.2718	6.5275	7.1592
q_{exp} (mol kg)$^{-1}$	0.026499	0.029079	0.030265	0.033194

Table 4
Thermodynamic parameters for the atrazine adsorption onto the BCC.

T (K)	K_e (-)	ΔG^0 (kJ mol^{-1})	ΔH^0 (kJ mol^{-1})	ΔS^0 (kJ mol^{-1} K^{-1})
298.150	115,231.0	-28.899	15.721	0.14920
308.150	123,164.0	-30.029		
318.150	169,323.0	-31.845		
328.150	197,824.0	-33.271		

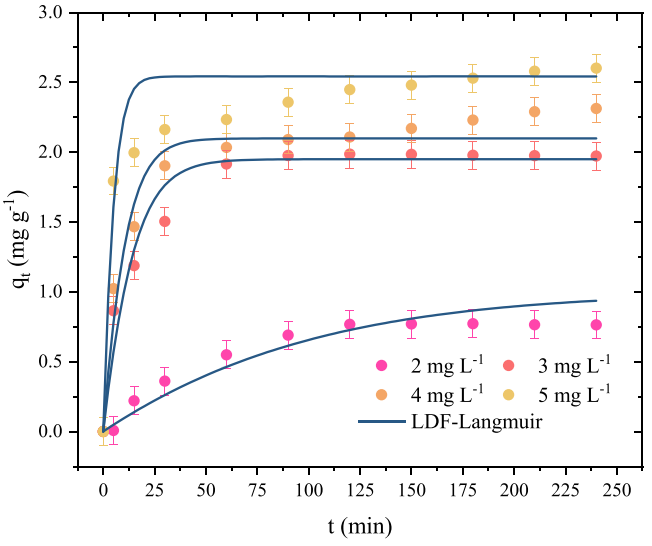

Fig. 7. Experimental and predicted data for the adsorption kinetics of atrazine on BCC.

adsorption tests on BCC. A spectrophotometer (UV mini 1240, Shimadzu) was used to measure the concentration of atrazine in the liquid phase at a wavelength of 222 nm, corresponding to the herbicide. An initial concentration of 5 mg L^{-1} atrazine in 20 mL was used for the dosage and pH effect studies, with the thermostatic agitator set to 150 rpm and 1 h. The BCC dosages of 0.5, 1.0, 1.5, 2, and 2.5 g L^{-1} were tested. The pH tested ranged from 2 to 10, and the atrazine solutions

Table 5
Estimated parameters for the LDF model.

Model	Atrazine initial concentration (mg L^{-1})			
	2	3	4	5
LDF				
q_{exp}(mg g^{-1})	0.76330	1.9721	2.3124	2.6019
q_{pred} (mg g^{-1})	0.83229	2.1213	2.0319	2.4662
k_{LDF}(s^{-1})	5.9011×10^{-5}	5.4626×10^{-4}	7.5601×10^{-4}	1.7655×10^{-3}
D_S (cm^2 s^{-1})	1.1866×10^{-8}	5.3105×10^{-8}	1.0393×10^{-7}	2.4898×10^{-5}
R^2	0.98367	0.9182	0.9413	0.9314
ARE (%)	14.030	14.862	9.0507	6.4210
MSR(mg g^{-1})^2	1.6072×10^{-3}	3.4628×10^{-2}	2.9504×10^{-2}	3.7945×10^{-2}

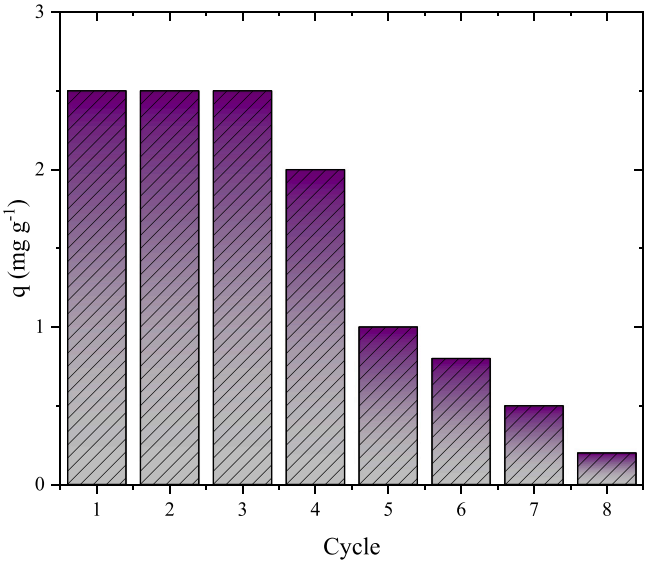

Fig. 8. BCC regeneration over eight cycles.

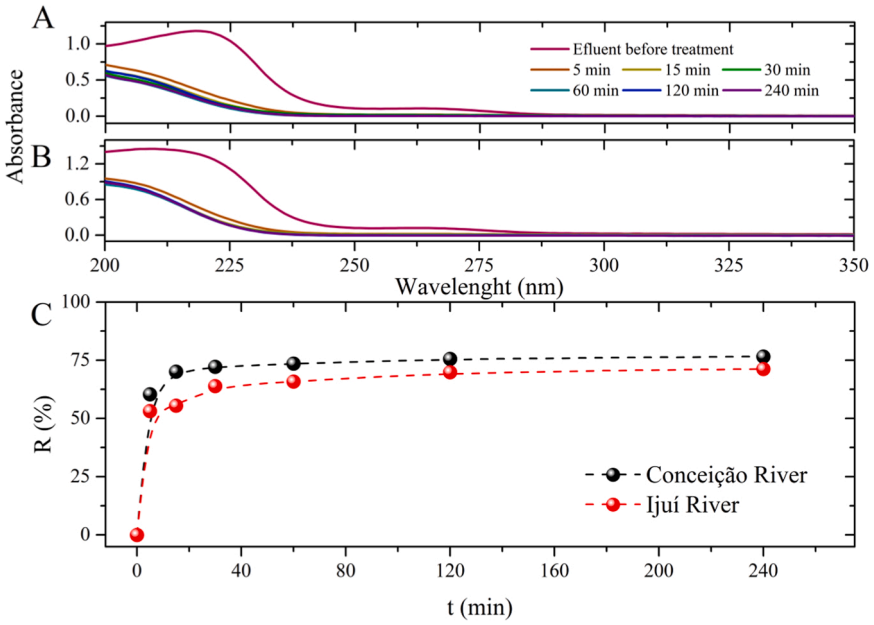

Fig. 9. Atrazine spectrum for the (A) Conceiç ão and (B) Ijuí river at different times, percentage of removal according to the river sample, and time (C).

were adjusted using HCl or NaOH solutions with 0.1 mol L^{-1} concentrations.

The isothermal and kinetic experiments were carried out using the best conditions of pH and dosage of BCC previously verified and a solution volume of 20 mL. Isothermal studies were carried out by varying the temperature in the system at 298, 308, 318, and 328 K for initial concentrations of 0, 5, 8, 10, 15, 18, and 20 mg L^{-1} of atrazine, kept under stirring at 150 rpm in a thermostatic bath. Kinetic curves were obtained at concentrations of 5, 4, 3, and 2 mg L^{-1} of atrazine. Samples were collected at 0, 5, 15, 30, 60, 90, 120, 150, 180, 210, and 240 min. Atrazine concentrations were determined by spectrophotometry. The percentage of pesticide removal (R, %), adsorption capacity at any time (qt, mg g^{-1}), and equilibrium adsorption capacity (q_e, mg g^{-1}) were calculated according to the supplementary material S2.

2.4. Isotherms and thermodynamic parameters

The Freundlich [26], Dubinin-Radushkevich [27], and Langmuir [28] models were chosen to be fitted to the equilibrium isotherms [29]. Then, according to the methodology proposed elsewhere [30], the thermodynamic parameters were estimated. These equations are listed in Supplementary Material S3 and S4, respectively.

2.5. Kinetic modeling

The linear driving force (LDF) model (Eq. 1) was chosen to describe the atrazine adsorption onto the BCC. This model considers that the rate of adsorption is dependent on the adsorption gradient between the maximum adsorption capacity and the adsorption capacity at any time [31]. In addition to that, the LDF parameters are related to the diffusion of the atrazine/BCC system. The derivation of the model is shown in Supplementary Material S5.

$$\frac{dq}{dt} = k_{LDF}\left(\frac{q_L K_L (C_0 - D_0 q)}{(1 + K_L (C_0 - D_0 q))} - q\right) \quad (1)$$

$$q\ (t = 0) = 0 \quad (1.1)$$

$$D_S = \frac{R_p{}^2 k_{LDF}}{15} \quad (2)$$

Where: q is the adsorption capacity (mg g^{-1}), k_{LDF} is the kinetic lumped parameter (min^{-1}), q_L is the Langmuir maximum adsorption capacity (mg g^{-1}), K_L is the Langmuir constant (L mg^{-1}), C_0 is the initial atrazine concentration (mg L^{-1}), D_0 is the adsorbent dosage (g L^{-1}), R_p is the radius of the adsorbent (cm), and D_s is the diffusion coefficient (cm^2 s^{-1}).

2.6. Parameter estimation and evaluation

The parameter estimations and LDF solutions were done using Matlab. The following built-in functions were chosen for the model parameters: *particleswarm*, *nlinfit*, *lsqnonlin*. Concerning the LDF solution, the *ode15s* was employed for solving the model. In addition, according to the Supplementary material (S5), the best model fit was evaluated.

2.7. Thermal regeneration and reuse

The regeneration tests were performed in cycles: first, the adsorbent loaded with atrazine was regenerated through heating. For this, the adsorbent was placed in the oven for 2 h at 300 ºC. This process should remove the atrazine from its boiling point (205 ºC). Second, 1.5 g L^{-1} of adsorbent was put in contact with atrazine solution (5 mg L^{-1}) and agitated for 4 h at room temperature (298 K) and constant agitation (150 rpm). After that, the atrazine concentration was measured through UV-Vis spectroscopy. This cycle was repeated eight times, always using the previously regenerated adsorbent.

2.8. Treatment of river water containing atrazine

As herbicides used in crops are frequently leached by rainwater into water resources, the performance of BCC in real river water samples was analyzed. The Ijuí river is a watercourse in the state of Rio Grande do Sul, while the Conceiç ão River is a tributary of the Ijuí River. Both are located close to large tracts of crops planted with various crops, mainly corn and soybeans. About 100 mL of sample from each river was contaminated with 5 mg L^{-1} of herbicide. Then, 1.5 g L^{-1} of BCC was added to the solution and stirred at 150 rpm. Samples were collected at 0, 5, 15, 30, 60, 120, and 240 min, then centrifuged. The percentage of removal (R, %) was estimated according to Eq. (3):

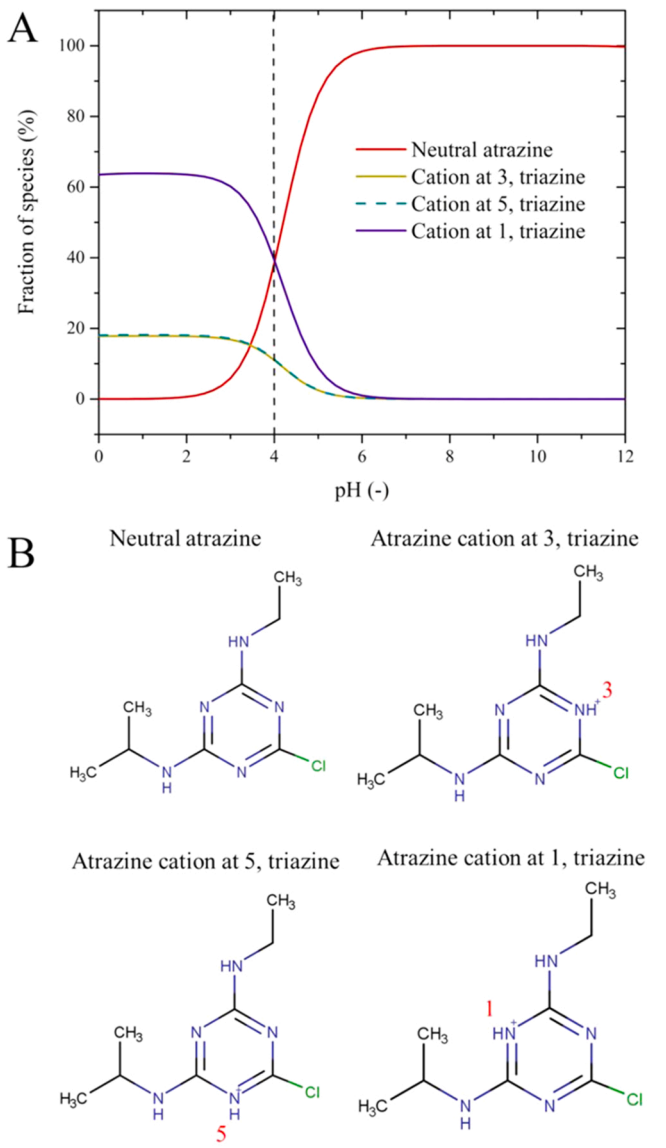

Fig. 10. Atrazine speciation diagram according to Marvin sketch pK_a estimations (A) and different atrazine ionic forms (B).

$$R = \left(1 - \frac{A_t}{A_0}\right) 100\% \quad (3)$$

A_0 is the area under the spectrum curve before the adsorption, and A_t is the area under the spectrum curve after the adsorption at different times.

3. Results and discussion

3.1. CBS and CBB characteristics

The scanning electron microscopy images for the CBS (A) and BCC (B) are depicted in Fig. 1. The CBS presents a typical morphology of wood-waste-derived biomass, with circular and well-defined structures common for *Cedrella fissilis*. However, after being subjected to pyrolysis up to 800 °C (BCC), the surface presented irregular and uneven shapes, containing new spaces/cavities randomly distributed in the material. Therefore, the structure before and after pyrolysis is defined according to the organic matter present in the biochar [32]. Sbizzaro et al. [33] found a similar behavior when preparing two biochars from bamboo. They observed that the increase in temperature from 350° to 550°C provided more cavities and irregularities on the material's surface, with greater porosity and, consequently, greater surface area. These new spaces are formed with increased production temperatures due to the release of volatile compounds and a more regular structure [34].

Regarding the textural characteristics, the BCC presented a specific surface area (Fig. 2a) of 27.96 m^2 g^{-1}, which is relatively low when compared to activated carbons [35,36], but high when compared to other existing biochars in the literature [37–39]. Furthermore, the N_2 adsorption isotherms showed a hysteresis loop in the region from 0.4 to 0.9, confirming the presence of mesopores [40]. According to the IUPAC classification, the BCC revealed type IV adsorption-desorption isotherms with a pore volume of 0.018 cm^3 g^{-1} and a pore diameter of 1.13 nm (Fig. 2b) characteristic of a mesoporous structure [41]. This pore volume value is close to that obtained by Hollister et al. [42], 0.006 cm^3 g^{-1} for corn husk biochar, and by Luo et al. [38], 0.008 cm^3 g^{-1} for corn cob biochar. The modification of the carbon structure of the BCC caused by the increase in temperature in the pyrolysis step results in changes in the textural characteristics, which can favor atrazine adsorption.

The energy-dispersive X-ray spectroscopy (EDS) results are presented in Table 1. It is possible to observe that the carbonization process increases the C % and decreases the O %. This behavior is expected for biochars and activated carbons, where the ratio of oxygen per carbon tends to decrease. Since, during the carbonization process, the hydroxyl groups tend to be broken. Similar results were also reported by Ahmad et al. [43] when studying the pyrolysis of peanut shells and by Peng et al. [44] for the biochar obtained from sugarcane bagasse.

The pH_{pzc} value of the biochar was found at 7.51. In this region, the pH shows the smallest variation. In the literature, it is possible to observe that the pH_{pzc} tends to increase as the pyrolysis temperature increases [45]. Therefore, biochars produced at lower temperatures may contain more acidic functional groups due to incomplete degradation [46,47]. As is the case in this study, biochars produced at higher temperatures have higher pH_{pzc} values and more basic functional groups [46,47]. This result agrees with the FT-IR spectra (Table 2), where a reduction of functional groups responsible for decreasing the surface charge was observed.

The main bands observed through the FTIR for CBS and BCC are presented in Table 2. The great vibrational elongation present at 3444 cm^{-1} is typical of the OH bond present in lignin and holocellulose [48]. At 1052 cm^{-1}, there is a CO elongation of the phenolic compounds found in lignin [25]. In BCC, the intensity of the bands at 3444 cm^{-1} decreases drastically, indicating that a dehydration reaction occurred in the cellulose after the pyrolysis process [49].

The XRD pattern revealed that both adsorbents do not have a crystalline structure due to the absence of sharp peaks. Broad peaks from 10° to 30° for CBS and from 15° to 30° for BCC were verified, confirming its lignocellulosic structure and indicating that the adsorbents are amorphous [48]. For BCC, peaks appearing around 40–50° corresponding to reflections of the disordered micrographic structure, which are characteristic of activated carbon, were also verified [44]. The XRD image can be found in Supplementary Material S6.

Fig. 3 shows the TGA curves for CBS and BCC. For CBS (black line), three well-defined weight loss regions can be visualized. The first stage occurs between 25 and 100 °C and is proportional to the surface water loss [45], corresponding to 7.5% of the total mass. In the second stage, from 290° to 400°C, around 60% of the total mass was lost. In this stage, the weight loss is relative to the reactions with cellulose and hemicellulose, which release volatile compounds. The final stage was from 400° to 800°C, and this weight loss could be relative to the lignin degradation or break of the carbonaceous skeleton. The residual weight of CBS was 13%. In parallel, only two weight loss stages were found for BCC (blue line). The first was from 25° to 490°C, where only 10% was lost. Again, this loss is relative to surface water and the degradation of some remaining functional groups after pyrolysis. The last step was from 490° to 800°C. This mass loss step is relative to the decomposition of the carbonaceous skeleton but was only 10%. The residual weight of BCC

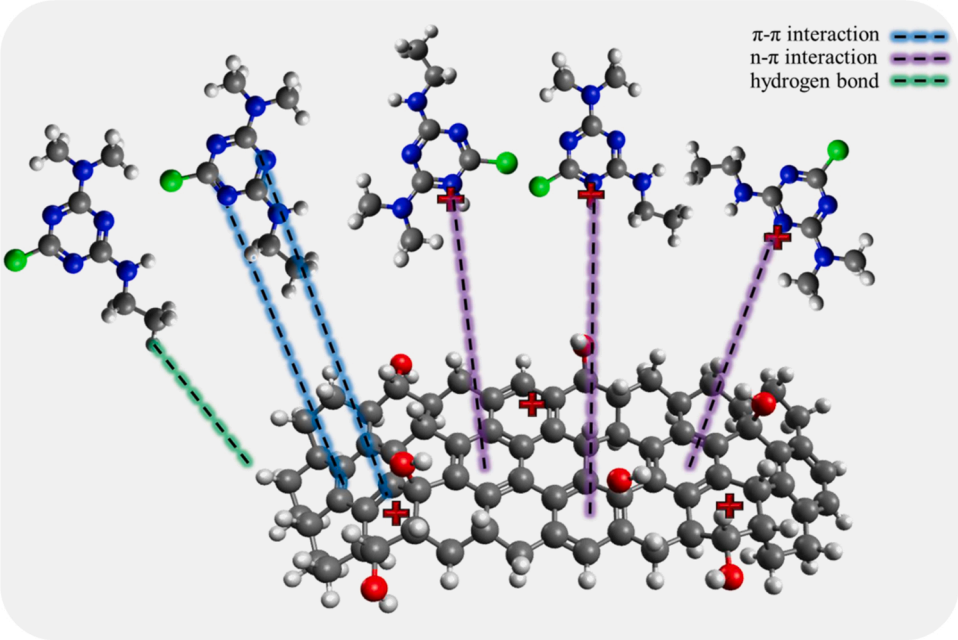

Fig. 11. Possible interactions in the atrazine adsorption on BCC at pH of 4.

was 78%. These profiles prove that pyrolysis generates biochar with high thermal stability.

3.2. Effects of biochar dosage and pH on the atrazine adsorption

The effect of the BCC dosage on the herbicide adsorption capacity and efficiency is shown in Fig. 4.

The increase in removal from 25% to 77% occurred when the dosage was increased from 0.5 to 2.5 g L^{-1} due to the greater number of adsorption sites. The dosage of 1.5 g L^{-1} (intersection of the curves) obtained excellent removal values (65%) and capacity (2.3 mg g^{-1}), which were fixed for the following studies. Finally, the adsorption capacity (q) values showed an inverse dependence on removal (R %). Values decreased from 2.6 to 1.6 mg g^{-1} when the adsorbent dose was increased from 0.5 to 2.5 g L^{-1} due to the superposition of adsorption sites at higher dosages.

Through Fig. 5, it is possible to observe that atrazine adsorption occurs at an acidic pH (between 2 and 4) since as the pH increases from 4 to 10, the capacity decreases drastically. In this pH range (2−4), BCC is protonated since its pH_{pzc} is 7.51. In parallel, atrazine is considered a weak base, with a pK_a at 4.20. At these pH conditions, a fraction of molecules is neutral, and a fraction is in a cationic form of triazine. In this sense, we can point out that the main adsorption interaction type depends less on electrostatic forces. The adsorption interactions are well detailed in the next sections. In the literature, it is possible to find other studies where atrazine adsorption is favored under acidic conditions [23,51,52]. As a result, the pH 4 was set for future experiments.

3.3. Adsorption isotherm and thermodynamics

The isothermal curves were determined (Fig. 6) to better understand the distribution of adsorbate between liquid and solid phases when equilibrium occurs. The four sequences of experimental data represent the relationship of the herbicide's adsorption capacity (q_{eq}) on the BCC under different concentrations (C_{eq}).

First, the shape of the isotherm is analyzed. The curves were convex, with an inclined portion at low C_e values, followed by a plateau. This shape is near to an "L2" type curve. The inclined portion reveals that the proposed adsorbent (BCC) is suitable since higher adsorption capacities coupled with low C_e values could be found. Besides, the plateau shows that the BCC surface was saturated. Concerning now the temperature effect, Fig. 6 reveals an endothermic profile. For example, at higher concentrations, the atrazine adsorption capacity on BCC increased from 5.71 to 7.15 mg g^{-1} with the temperature increase. This behavior may be related to the increase in the energy exchange during the process [53]. Salomón et al. [14] also observed that at the same temperature interval, the atrazine adsorption capacity increased from 194.2 to 211.5 mg g^{-1}, using activated carbon from fruit residues. The same behavior was reported by Alahabadi and Moussavi [54] using activated charcoal prepared from the dry stem of the *Calligonum comosum* plant when the temperature was raised from 283 to 313 K.

The isothermal data fitted the Langmuir, Freundlich, and Dubinin-Radushkevich models (Table 3). The best model was defined through the analysis of statistical coefficients. The Langmuir model provided the best fit, with the highest values of determination coefficient (R^2 >0.9870), adjusted coefficient of determination (R^2_{adj}> 0.9805), and lowest values of ARE (<5.28%) and MSR (<0.099 (mg g^{-1})^2). Furthermore, the capacity values of the model are in agreement with the experimental values, increasing with increasing temperature, reaching a maximum capacity of 7.68 mg g^{-1} at 328 K. It was also observed that the K_L and q_L parameters were directly proportional to temperature, indicating the adsorbate/adsorbent affinity and adsorption capacity were favored at 328 K [25]. In the literature, it is possible to observe several adsorbents that present better adjustment to the Langmuir isotherm in removing atrazine, indicating that herbicide molecules tend to adhere to the surface of the adsorbent through the formation of monolayers, related to homogeneous surfaces [23,33,54–60].

By analyzing the adsorption performance of BCC with other adsorbents present in the literature on atrazine removal, it was possible to observe a good performance of BCC. Salvestrini et al. [51], when using Acid-activated zeolite-rich tufts, they reached a maximum capacity of 1.1 mg g^{-1}, with a concentration varying between 5 and 15 mg L^{-1}. Yue et al. [59] reached a capacity of 5.58 mg g^{-1} for the concentration range of 5–20 mg L^{-1} using rice husk as adsorbent. Toledo et al. [61] used bentonite modified with benzyl-chloride-octadecyl-dimethyl-ammonium and reached a capacity of 4.24 mg g^{-1} for a concentration of 10–20 mg L^{-1} of atrazine. However, it is also possible to observe adsorbents with higher adsorption capacity values for higher values of

concentration ranges. Wei et al. [18,60] reached maximum capacities of 46.3 and 222.22 mg g^{-1}, for minimum and maximum concentrations of 60–110 mg L^{-1}, using activated carbon derived from apricot peel and coal-based activated carbon modified with sodium dodecylbenzene sulfonate, respectively.

Table 4 shows the thermodynamic data of atrazine adsorption on BCC. It can be seen that K_e values increased with temperature, and consequently, ΔG^0 values were more negative. This trend indicates that the adsorbate/adsorbent product formation favored 328 K and confirmed the process's spontaneity. Besides, the positive ΔS^0 indicates that some rearrangements occurred on the BCC surface during atrazine adsorption. The positive ΔH^0 sign confirms that atrazine adsorption on BCC was endothermic. The ΔH^0 value of 15.72 kJ mol^{-1} indicates that physical interactions are involved in atrazine adsorption, specifically Van der Waals interactions or hydrogen bonds, since the value was less than 20 kJ mol^{-1} [62]. This find is consistent with the pH effect, where electrostatic forces were discarded.

3.4. Kinetics and application of the LDF model

Fig. 7 illustrates the kinetic curves of the BCC/atrazine system and represents the time required for the system to reach equilibrium at four concentrations at room temperature (298 K). It was observed that as the concentration was increased, the faster the system came to equilibrium. Thus, the equilibrium was concentration-dependent, being 180, 120, 90, and 60 min for the concentrations of 2, 3, 4, and 4 mg L^{-1}, respectively. As the concentration increased, an increase in the adsorption capacity was also observed, being 0.77, 1.98, 2.09, and 2.3 mg g^{-1}. The behavior was observed mainly for the initial concentrations of 3, 4, and 5 mg L^{-1}, where the capacity increases rapidly in the first minutes, and then the rate decays until reaching equilibrium. A single but suitable explanation for this trend is that the BCC surface is free in the first minutes, causing the molecules to be rapidly adsorbed. Over time, the surface becomes overloaded as where the adsorbate molecules slowly occupy the few available places [63,64].

The linear driving force (LDF) model was applied to the experimental data (Table 5). According to the good values of the statistical parameters ($R^2 \geq 0.9613$; MSR ≤ 0.0379 (mg $g^{-1})^2$, ARE$\leq$ 14.86%), the LDF force model can be used to represent the BCC/atrazine system. Added to this, the capacity values of the model are in agreement with the values obtained experimentally. Furthermore, the mass transfer coefficient (K_{LDF}) and the diffusion coefficient (Ds) increased with the initial concentration. This behavior confirms that the atrazine adsorption was faster at higher initial concentrations. This effect is related to increasing the atrazine concentration gradient, which leads to higher intraparticle mass transfer and external mass transfer rates [65]. This behavior was also reported by Lazarotto et al. [13] and Franco et al. [65] when using activated carbons to remove 2,4-dichlorophenoxyacetic and phenol, respectively.

3.5. Regeneration and reuse of BCC

The material's regeneration performance is a major advantage for adsorption technology in terms of economics and sustainability for industrial applications. Therefore, just as the retention of adsorbate is important, its regeneration capacity must also be analyzed. Fig. 8 shows the BCC adsorbent regeneration cycles based on the adsorption capacity achieved in each of them. The adsorbent still presents good adsorption in the first three cycles. From the first cycle to the third, the material maintained practically the same efficiency. However, there is a decrease in adsorption capacity from the third cycle. This trend occurred because even though BCC has thermal stability, some adsorption sites on the surface are degraded during consecutive cycles of thermal desorption.

3.6. River water treatment

The BCC removal efficiency was tested using water from two rivers without any treatment. The two samples containing 5 mg L^{-1} of atrazine were treated with 1.5 g L^{-1} of BCC. The spectrum for the Conceiç ão and Ijuí rivers at different times and the percentage of removal according to time are displayed in Fig. 9.

The first aspect to be noticed is that the BCC could adsorb the atrazine from different river samples. Second, equilibrium was achieved in 120 min for both samples, reaching a percentage of removal of 76.58% and 71.29% for the Conceiç ão and Ijuí rivers, respectively. Thus, it is confirmed that BCC has potential atrazine removal in real water samples. In the study by Lazarotto et al. [13], the authors contaminated a water sample from the Jacuí River (Agudo, Rio Grande do Sul, Brazil) with 10 mg L^{-1} of the 2,4-D herbicide. They verified the removal of 70% using activated charcoal. In the study by Salomon et al.[14], reduced the atrazine concentration from 4.7 μg L^{-1} to 0.70 μg L^{-1} in the Jacuí River water, using activated charcoal.

3.7. Adsorption mechanism proposal

Considering the results from the characterization (FT-IR, EDS, pH_{pzc}), solution pH, pK_a, speciation of the atrazine, and the thermodynamic parameters, it is possible to suggest an adsorption mechanism. The first step is the proposal of the surface of the adsorbent. From the FT-IR before and after the pyrolysis step is expected that the adsorbent surface is mainly constituted of OH and C═C groups, forming aromatic rings and carboxylic groups. In addition to that, for every eight carbons, there is one oxygen. Besides that, the pH_{pzc} was found to be 7.51, meaning that the surface of the BCC will tend to present a positive surface since the optimum pH was found to be 4. Second, the solution pH and pK_a of the atrazine are important to understand how the atrazine is found in the solution. The atrazine is a molecule without oxygen and a triazine (nitrogen/carbon aromatic group), meaning that atrazine has several different ionic states. At pH 4, the atrazine molecules have 4 different states (Fig. 10), 38.53% of the atrazine is found in the neutral form; the other percentage is found in the cationic form, divided into three different states: 39.31% of the atrazine is found with nitrogen cation at position 1 of the triazine group; 22% corresponds to the atrazine found with nitrogen cation at positions 3 and 5 of the triazine group (each state is 11%). Last, the enthalpy value indicates that the adsorption has a physical nature. This pattern indicates that the adsorption mainly occurs due to hydrogen bonding, π–π or n–π interactions [66,67].

It should be noted that 61.3% of the atrazine will have a positive charge, and the remaining is found in neutral form. Since at low pH, the surface of the adsorbent may have a positive charge, it is expected that electrostatic force should not occur. However, due to the possibility of the aromatic ring on the surface and the triazine of the atrazine, it is expected that n–π interactions could occur in the form of cation–π interactions. Besides that, traditional hydrogen bonds between the neutral atrazine and adsorbent are also expected. A summary of the possible interactions between the BCC and the atrazine is shown in Fig. 11.

4. Conclusions

The application of residual sawdust from the wood industry chain of the species *Cedrella fissilis* was promising for the production of porous biochar. The developed adsorbent efficiently removed the atrazine herbicide in a synthetic mixture and a contaminated river water sample. Adsorption was favored under acidic conditions for an ideal dosage of 1.5 g L^{-1} of biochar and a temperature of 328 K. The maximum capacity obtained by the Langmuir isotherm was 7.68 mg g^{-1}. Thermodynamic parameters confirmed the endothermic nature. The LDF kinetic model satisfactorily represented the experimental data, obtaining a diffusion coefficient ranging from 5.31×10^{-8} to 2.49×10^{-5} cm^2 s^{-1}. Besides, the biochar can be reused in up to 3 cycles. In water samples from two rivers

contaminated with atrazine, biochar obtained maximum removals higher than 70% in a time of 120 min. Finally, it is suggested that n–π, π –π and H-bonds were the main interactions between atrazine-biochar.

CRediT authorship contribution statement

Paola T. Hernandes: Conceptualization, Investigation, Resources, Writing – original draft, Methodology, Formal analysis. **Dison S. P. Franco:** Conceptualization, Investigation, Resources, Writing – original draft, Methodology, Formal analysis. **Jordana Georgin:** Methodology, Formal analysis, Writing – review & editing. **Nina P. G. Salau:** Conceptualization, Investigation, Resources, Writing – original draft, Methodology, Formal analysis. **Guilherme L. Dotto:** Supervision, Project administration, Funding acquisition, Conceptualization, Writing – review & editing.

Declaration of Competing Interest

The authors declare that they have no known competing financial interests or personal relationships that could have appeared to influence the work reported in this paper.

Appendix A. Supporting information

Supplementary data associated with this article can be found in the online version at doi:10.1016/j.jece.2022.107408.

References

[1] T.B. Hayes, A. Collins, M. Lee, M. Mendoza, N. Noriega, A.A. Stuart, A. Vonk, Hermaphroditic, demasculinized frogs after exposure to the herbicide atrazine at low ecologically relevant doses, Proc. Natl. Acad. Sci. U.S.A. 99 (2002) 5476–5480, https://doi.org/10.1073/pnas.082121499.

[2] J.P. Lasserre, F. Fack, D. Revets, S. Planchon, J. Renaut, L. Hoffmann, A.C. Gutleb, C.P. Muller, T. Bohn, Effects of the endocrine disruptors atrazine and PCB 153 on the protein expression of MCF-7 human cells, J. Proteome Res. 8 (2009) 5485–5496, https://doi.org/10.1021/pr900480f.

[3] S. Rostami, S. Jafari, Z. Moeini, M. Jaskulak, L. Keshtgar, A. Badeenezhad, A. Azhdarpoor, M. Rostami, K. Zorena, M. Dehghani, Current methods and technologies for degradation of atrazine in contaminated soil and water: a review, Environ. Technol. Innov. 24 (2021), 102019, https://doi.org/10.1016/j.eti.2021.102019.

[4] M. Shirmardi, N. Alavi, E.C. Lima, A. Takdastan, A.H. Mahvi, A.A. Babaei, Removal of atrazine as an organic micro-pollutant from aqueous solutions: a comparative study, Process Saf. Environ. Prot. 103 (2016) 23–35, https://doi.org/10.1016/j.psep.2016.06.014.

[5] M. Graymore, F. Stagnitti, G. Allinson, Impacts of atrazine in aquatic ecosystems, Environ. Int. 26 (2001) 483–495, https://doi.org/10.1016/S0160-4120(01)00031-9.

[6] G.W. Stratton, Effects of the herbicide atrazine and its degradation products, alone and in combination, on phototrophic microorganisms, Arch. Environ. Contam. Toxicol. 13 (1984) 35–42, https://doi.org/10.1007/BF01055644.

[7] Z. Shamsollahi, A. Partovinia, Recent advances on pollutants removal by rice husk as a bio-based adsorbent: a critical review, J. Environ. Manag. 246 (2019) 314–323, https://doi.org/10.1016/j.jenvman.2019.05.145.

[8] S. Sun, J. Zhu, Z. Zheng, J. Li, M. Gan, Biosynthesis of β-cyclodextrin modified Schwertmannite and the application in heavy metals adsorption, Powder Technol. 342 (2019) 181–192, https://doi.org/10.1016/j.powtec.2018.09.072.

[9] H. Pang, Z. Diao, X. Wang, Y. Ma, S. Yu, H. Zhu, Z. Chen, B. Hu, J. Chen, X. Wang, Adsorptive and reductive removal of U(VI) by Dictyophora indusiate-derived biochar supported sulfide NZVI from wastewater, Chem. Eng. J. 366 (2019) 368–377, https://doi.org/10.1016/j.cej.2019.02.098.

[10] J. Qu, Y. Yuan, Q. Meng, G. Zhang, F. Deng, L. Wang, Y. Tao, Z. Jiang, Y. Zhang, Simultaneously enhanced removal and stepwise recovery of atrazine and Pb(II) from water using β–cyclodextrin functionalized cellulose: characterization, adsorptive performance and mechanism exploration, J. Hazard. Mater. 400 (2020), 123142, https://doi.org/10.1016/j.jhazmat.2020.123142.

[11] L. Wu, B. Li, M. Liu, Influence of aromatic structure and substitution of carboxyl groups of aromatic acids on their sorption to biochars, Chemosphere 210 (2018) 239–246, https://doi.org/10.1016/j.chemosphere.2018.07.003.

[12] Y. Dai, N. Zhang, C. Xing, Q. Cui, Q. Sun, The adsorption, regeneration and engineering applications of biochar for removal organic pollutants: a review, Chemosphere 223 (2019) 12–27, https://doi.org/10.1016/j.chemosphere.2019.01.161.

[13] J.S. Lazarotto, K. da Boit Martinello, J. Georgin, D.S.P. Franco, M.S. Netto, D.G. A. Piccilli, L.F.O. Silva, E.C. Lima, G.L. Dotto, Preparation of activated carbon from the residues of the mushroom (Agaricus bisporus) production chain for the adsorption of the 2,4-dichlorophenoxyacetic herbicide, J. Environ. Chem. Eng. 9 (2021), https://doi.org/10.1016/j.jece.2021.106843.

[14] Y.L. Salomón, J. Georgin, D.S.P. Franco, M.S. Netto, D.G.A. Piccilli, E.L. Foletto, D. Pinto, M.L.S. Oliveira, G.L. Dotto, Adsorption of atrazine herbicide from water by Diospyros kaki fruit waste activated carbon, J. Mol. Liq. (2021), https://doi.org/10.1016/j.molliq.2021.117990.

[15] H.M. Mohd Noor Hazrin, A. Lim, C. Li, J.J. Chew, J. Sunarso, Adsorption of 2,4-dichlorophenoxyacetic acid onto oil palm trunk-derived activated carbon: isotherm and kinetic studies at acidic, ambient condition, Mater. Today Proc. (2021) 1–6, https://doi.org/10.1016/j.matpr.2021.09.461.

[16] K. Rambabu, J. Alyammahi, G. Bharath, A. Thanigaivelan, N. Sivarajasekar, F. Banat, Nano-activated carbon derived from date palm coir waste for efficient sequestration of noxious 2,4-dichlorophenoxyacetic acid herbicide, Chemosphere 282 (2021), 131103, https://doi.org/10.1016/j.chemosphere.2021.131103.

[17] A. Pandiarajan, R. Kamaraj, S.S.S. Vasudevan, S.S.S. Vasudevan, OPAC (orange peel activated carbon) derived from waste orange peel for the adsorption of chlorophenoxyacetic acid herbicides from water: adsorption isotherm, kinetic modelling and thermodynamic studies, Bioresour. Technol. 261 (2018) 329–341, https://doi.org/10.1016/j.biortech.2018.04.005.

[18] X. Wei, Z. Wu, Z. Wu, B.C. Ye, Adsorption behaviors of atrazine and Cr(III) onto different activated carbons in single and co-solute systems, Powder Technol. 329 (2018) 207–216, https://doi.org/10.1016/j.powtec.2018.01.060.

[20] L. Sellaoui, L.F.O. Silva, M. Badawi, J. Ali, N. Favarin, G.L. Dotto, A. Erto, Z. Chen, Adsorption of ketoprofen and 2- nitrophenol on activated carbon prepared from winery wastes: a combined experimental and theoretical study, J. Mol. Liq. 333 (2021), https://doi.org/10.1016/j.molliq.2021.115906.

[21] L. Sellaoui, F. Dhaouadi, Z. Li, T.R.S. Cadaval, A.V. Igansi, L.A.A. Pinto, G.L. Dotto, A. Bonilla-Petriciolet, D. Pinto, Z. Chen, Implementation of a multilayer statistical physics model to interpret the adsorption of food dyes on a chitosan film, J. Environ. Chem. Eng. 9 (2021), 105516, https://doi.org/10.1016/j.jece.2021.105516.

[22] H. Xue, X. Wang, Q. Xu, F. Dhaouadi, L. Sellaoui, M.K. Seliem, A. Ben Lamine, H. Belmabrouk, A. Bajahzar, A. Bonilla-Petriciolet, Z. Li, Q. Li, Adsorption of methylene blue from aqueous solution on activated carbons and composite prepared from an agricultural waste biomass: a comparative study by experimental and advanced modeling analysis, Chem. Eng. J. 430 (2022), https://doi.org/10.1016/j.cej.2021.132801.

[23] X. Wei, Z.Z.Z.Z. Wu, Z.Z.Z.Z. Wu, B.C. Ye, Adsorption behaviors of atrazine and Cr (III) onto different activated carbons in single and co-solute systems, Powder Technol. 329 (2018) 207–216, https://doi.org/10.1016/j.powtec.2018.01.060.

[24] J. Georgin, D.S.P. Franco, M.S. Netto, D.G.A. Piccilli, E.L. Foletto, G.L. Dotto, Adsorption investigation of 2,4-D herbicide on acid-treated peanut (Arachis hypogaea) skins, Environ. Sci. Pollut. Res. 28 (2021) 36453–36463, https://doi.org/10.1007/s11356-021-12813-0.

[25] J. Georgin, D.S.P.P.D.S.P.D.S.P. Franco, P. Grassi, D. Tonato, D.G.A.A.D.G. A. Piccilli, L. Meili, G.L.G.L.G.L.G.L.G.L. Dotto, Potential of Cedrella fissilis bark as an adsorbent for the removal of red 97 dye from aqueous effluents, Environ. Sci. Pollut. Res. 26 (2019) 19207–19219, https://doi.org/10.1007/s11356-019-05321-9.

[26] H. Freundlich, Über die adsorption in lösungen, Z. Phys. Chem. 57U (1907), https://doi.org/10.1515/zpch-1907-5723.

[27] M.M. Dubinin, V.A. Astakhov, B.P. Bering, V.A. Gordeeva, M.M. Dubinin, L. I. Efimova, V.V. Serpinskii, Development of concepts of the volume filling of micropores in the adsorption of gases and vapors by microporous adsorbents - communication 4. Differential heats and entropies of adsorption, Bull. Acad. Sci. USSR Div. Chem. Sci. 20 (1971) 17–22, https://doi.org/10.1007/BF00849310.

[28] I. Langmuir, The adsorption of gases on plane surfaces of glass, mica and platinum, J. Am. Chem. Soc. 40 (1918) 1361–1403, https://doi.org/10.1021/ja02242a004.

[29] É.C. Lima, M.H. Dehghani, A. Guleria, F. Sher, R.R. Karri, G.L. Dotto, H.N. Tran, Adsorption: fundamental aspects and applications of adsorption for effluent treatment, in: M. Hadi Dehghani, R. Karri, E. Lima (Eds.), Green Technol. Defluoridation Water, Elsevier, 2021, pp. 41–88, https://doi.org/10.1016/b978-0-323-85768-0.00004-x.

[30] E.C. Lima, A. Hosseini-Bandegharaei, J.C. Moreno-Piraján, I. Anastopoulos, A critical review of the estimation of the thermodynamic parameters on adsorption equilibria. Wrong use of equilibrium constant in the Van't Hoof equation for calculation of thermodynamic parameters of adsorption, J. Mol. Liq. 273 (2019) 425–434, https://doi.org/10.1016/j.molliq.2018.10.048.

[31] E. Glueckauf, Theory of chromatography. Part 10.—Formulæ for diffusion into spheres and their application to chromatography, Trans. Faraday Soc. 51 (1955) 1540–1551, https://doi.org/10.1039/TF9555101540.

[32] D. Rehrah, R.R. Bansode, O. Hassan, M. Ahmedna, Physico-chemical characterization of biochars from solid municipal waste for use in soil amendment, J. Anal. Appl. Pyrolysis 118 (2016) 42–53, https://doi.org/10.1016/j.jaap.2015.12.022.

[33] M. Sbizzaro, S. César Sampaio, R. Rinaldo dos Reis, F. de Assis Beraldi, D. Medina Rosa, C. Maria Branco de Freitas Maia, C. Saramago de Carvalho Marques dos Santos Cordovil, C. Tillvitz do Nascimento, E. Antonio da Silva, C. Eduardo Borba, Effect of production temperature in biochar properties from bamboo culm and its influences on atrazine adsorption from aqueous systems, J. Mol. Liq. 343 (2021), 117667, https://doi.org/10.1016/j.molliq.2021.117667.

[34] R. Goswami, J. Shim, S. Deka, D. Kumari, R. Kataki, M. Kumar, Characterization of cadmium removal from aqueous solution by biochar produced from Ipomoea fistulosa at different pyrolytic temperatures, Ecol. Eng. 97 (2016) 444–451, https://doi.org/10.1016/j.ecoleng.2016.10.007.

[35] D. Xia, F. Tan, C. Zhang, X. Jiang, Z. Chen, H. Li, Y. Zheng, Q. Li, Y. Wang, ZnCl 2 -activated biochar from biogas residue facilitates aqueous As(III) removal, Appl. Surf. Sci. 377 (2016) 361–369, https://doi.org/10.1016/j.apsusc.2016.03.109.
[36] A. Cougnaud, C. Faur, P. Le Cloirec, Removal of pesticides from aqueous solution: quantitative relationship between activated carbon characteristics and adsorption properties, Environ. Technol. 26 (2005) 857–866, https://doi.org/10.1080/09593332608618497.
[37] C. Zhao, J. Ma, Z. Li, H. Xia, H. Liu, Y. Yang, Highly enhanced adsorption performance of tetracycline antibiotics on KOH-activated biochar derived from reed plants, RSC Adv. 10 (2020) 5066–5076, https://doi.org/10.1039/c9ra09208k.
[38] M. Luo, H. Lin, Y. He, Y. Zhang, The influence of corncob-based biochar on remediation of arsenic and cadmium in yellow soil and cinnamon soil, Sci. Total Environ. 717 (2020), 137014, https://doi.org/10.1016/j.scitotenv.2020.137014.
[39] C. Lammirato, A. Miltner, M. Kaestner, Effects of wood char and activated carbon on the hydrolysis of cellobiose by β-glucosidase from Aspergillus niger, Soil Biol. Biochem. 43 (2011) 1936–1942, https://doi.org/10.1016/j.soilbio.2011.05.021.
[40] Z. Li, Y. Jin, T. Chen, F. Tang, J. Cai, J. Ma, Trimethylchlorosilane modified activated carbon for the adsorption of VOCs at high humidity, Sep. Purif. Technol. 272 (2021), 118659, https://doi.org/10.1016/j.seppur.2021.118659.
[41] M. Thommes, K. Kaneko, A.V. Neimark, J.P. Olivier, F. Rodriguez-Reinoso, J. Rouquerol, K.S.W. Sing, Physisorption of gases, with special reference to the evaluation of surface area and pore size distribution (IUPAC Technical Report), Pure Appl. Chem. 87 (2015) 1051–1069, https://doi.org/10.1515/pac-2014-1117.
[42] C.C. Hollister, J.J. Bisogni, J. Lehmann, Ammonium, nitrate, and phosphate sorption to and solute leaching from biochars prepared from corn stover (Zea mays L.) and oak wood (Quercus spp.), J. Environ. Qual. 42 (2013) 137–144, https://doi.org/10.2134/jeq2012.0033.
[43] M. Ahmad, S.S. Lee, X. Dou, D. Mohan, J.K. Sung, J.E. Yang, Y.S. Ok, Effects of pyrolysis temperature on soybean stover- and peanut shell-derived biochar properties and TCE adsorption in water, Bioresour. Technol. 118 (2012) 536–544, https://doi.org/10.1016/j.biortech.2012.05.042.
[44] P. Peng, Y.H. Lang, X.M. Wang, Adsorption behavior and mechanism of pentachlorophenol on reed biochars: PH effect, pyrolysis temperature, hydrochloric acid treatment and isotherms, Ecol. Eng. 90 (2016) 225–233, https://doi.org/10.1016/j.ecoleng.2016.01.039.
[45] Z. Mahdi, A. El Hanandeh, Q. Yu, Influence of pyrolysis conditions on surface characteristics and methylene blue adsorption of biochar derived from date seed biomass, Waste Biomass Valoriz. 8 (2017) 2061–2073, https://doi.org/10.1007/s12649-016-9714-y.
[46] B. Zhao, D. O'Connor, J. Zhang, T. Peng, Z. Shen, D.C.W.W. Tsang, D. Hou, Effect of pyrolysis temperature, heating rate, and residence time on rapeseed stem derived biochar, J. Clean. Prod. 174 (2018) 977–987, https://doi.org/10.1016/j.jclepro.2017.11.013.
[47] M. Keiluweit, P.S. Nico, M.G. Johnson, M. Kleber, Dynamic molecular structure of plant biomass-derived black carbon(Biochar), Environ. Sci. Technol. 44 (2010) 1247–1253, https://doi.org/10.1021/es9031419.
[48] L. Meili, P.V.S. Lins, M.T. Costa, R.L. Almeida, A.K.S. Abud, J.I. Soletti, G.L. Dotto, E.H. Tanabe, L. Sellaoui, S.H.V. Carvalho, A. Erto, Adsorption of methylene blue on agroindustrial wastes: experimental investigation and phenomenological modelling, Prog. Biophys. Mol. Biol. 141 (2019) 60–71, https://doi.org/10.1016/j.pbiomolbio.2018.07.011.
[49] J. Zhou, W. Zhu, J. Yu, H. Zhang, Y. Zhang, X. Lin, X. Luo, Highly selective and efficient removal of fluoride from ground water by layered Al-Zr-La Tri-metal hydroxide, Appl. Surf. Sci. 435 (2018) 920–927, https://doi.org/10.1016/j.apsusc.2017.11.108.
[51] S. Salvestrini, P. Sagliano, P. Iovino, S. Capasso, C. Colella, Atrazine adsorption by acid-activated zeolite-rich tuffs, Appl. Clay Sci. 49 (2010) 330–335, https://doi.org/10.1016/j.clay.2010.04.008.
[52] J. Lladó, C. Lao-Luque, B. Ruiz, E. Fuente, M. Solé-Sardans, A.D. Dorado, Role of activated carbon properties in atrazine and paracetamol adsorption equilibrium and kinetics, Process Saf. Environ. Prot. 95 (2015) 51–59, https://doi.org/10.1016/j.psep.2015.02.013.
[53] E.M. Cuerda-Correa, J.R. Domínguez-Vargas, F.J. Olivares-Marín, J.B. de Heredia, On the use of carbon blacks as potential low-cost adsorbents for the removal of non-steroidal anti-inflammatory drugs from river water, J. Hazard. Mater. 177 (2010) 1046–1053, https://doi.org/10.1016/j.jhazmat.2010.01.026.
[54] A. Alahabadi, G. Moussavi, Preparation, characterization and atrazine adsorption potential of mesoporous carbonate-induced activated biochar (CAB) from Calligonum Comosum biomass: parametric experiments and kinetics, equilibrium and thermodynamic modeling, J. Mol. Liq. 242 (2017) 40–52, https://doi.org/10.1016/j.molliq.2017.06.116.
[55] M.B. Chabalala, M.Z. Al-Abri, B.B. Mamba, E.N. Nxumalo, Mechanistic aspects for the enhanced adsorption of bromophenol blue and atrazine over cyclodextrin modified polyacrylonitrile nanofiber membranes, Chem. Eng. Res. Des. 169 (2021) 19–32, https://doi.org/10.1016/j.cherd.2021.02.010.
[56] Y. Cao, S. Jiang, Y. Zhang, J. Xu, L. Qiu, L. Wang, Investigation into adsorption characteristics and mechanism of atrazine on nano-MgO modified fallen leaf biochar, J. Environ. Chem. Eng. 9 (2021), 105727, https://doi.org/10.1016/j.jece.2021.105727.
[57] E.A. Allam, A.S.M. Ali, R.M. Elsharkawy, M.E. Mahmoud, Framework of nano metal oxides N-NiO@N-Fe3O4@N-ZnO for adsorptive removal of atrazine and bisphenol-A from wastewater: kinetic and adsorption studies, Environ. Nanotechnol. Monit. Manag. 16 (2021), 100481, https://doi.org/10.1016/j.enmm.2021.100481.
[58] M. Bayati, M. Numaan, A. Kadhem, Z. Salahshoor, S. Qasim, H. Deng, J. Lin, Z. Yan, C.H. Lin, M. Fidalgo De Cortalezzi, Adsorption of atrazine by laser induced graphitic material: an efficient, scalable and green alternative for pollution abatement, J. Environ. Chem. Eng. 8 (2020), 104407, https://doi.org/10.1016/j.jece.2020.104407.
[59] L. Yue, C.J. Ge, D. Feng, H. Yu, H. Deng, B. Fu, Adsorption–desorption behavior of atrazine on agricultural soils in China, J. Environ. Sci. 57 (2017) 180–189, https://doi.org/10.1016/j.jes.2016.11.002.
[60] X. Wei, Z. Wu, C. Du, Z. Wu, B.C. Ye, G. Cravotto, Enhanced adsorption of atrazine on a coal-based activated carbon modified with sodium dodecyl benzene sulfonate under microwave heating, J. Taiwan Inst. Chem. Eng. 77 (2017) 257–262, https://doi.org/10.1016/j.jtice.2017.04.004.
[61] H.P. Toledo-Jaldin, A. Blanco-Flores, V. Sánchez-Mendieta, O. Martín-Hernández, Influence of the chain length of surfactant in the modification of zeolites and clays. Removal of atrazine from water solutions, Environ. Technol. 39 (2018) 2679–2690, https://doi.org/10.1080/09593330.2017.1365097.
[62] F.M. Machado, C.P. Bergmann, T.H.M. Fernandes, E.C. Lima, B. Royer, T. Calvete, S.B. Fagan, Adsorption of Reactive Red M-2BE dye from water solutions by multi-walled carbon nanotubes and activated carbon, J. Hazard. Mater. 192 (2011) 1122–1131, https://doi.org/10.1016/j.jhazmat.2011.06.020.
[63] J. Georgin, D.S.P. Franco, M. Schadeck Netto, D. Allasia, E.L. Foletto, L.F. S. Oliveira, G.L. Dotto, Transforming shrub waste into a high-efficiency adsorbent: application of Physalis peruvian chalice treated with strong acid to remove the 2,4-dichlorophenoxyacetic acid herbicide, J. Environ. Chem. Eng. 9 (2021), 104574, https://doi.org/10.1016/j.jece.2020.104574.
[64] J. Georgin, D.S.P. Franco, M.S. Netto, Y.L.O. de Salomón, D.G.A. Piccilli, E. L. Foletto, G.L. Dotto, Adsorption and mass transfer studies of methylene blue onto comminuted seedpods from Luehea divaricata and Inga laurina, Environ. Sci. Pollut. Res. (2021), https://doi.org/10.1007/s11356-020-11957-9.
[65] D.S.P. Franco, J. Georgin, M.S. Netto, D. Allasia, M.L.S. Oliveira, E.L. Foletto, G. L. Dotto, Highly effective adsorption of synthetic phenol effluent by a novel activated carbon prepared from fruit wastes of the Ceiba speciosa forest species, J. Environ. Chem. Eng. 9 (2021), 105927, https://doi.org/10.1016/j.jece.2021.105927.
[66] P.S. Thue, C.S. Umpierres, E.C. Lima, D.R. Lima, F.M. Machado, G.S. dos Reis, R. S. da Silva, F.A. Pavan, H.N. Tran, Single-step pyrolysis for producing magnetic activated carbon from tucumã (Astrocaryum aculeatum) seed and nickel(II) chloride and zinc(II) chloride. Application for removal of nicotinamide and propanolol, J. Hazard. Mater. 398 (2020), 122903, https://doi.org/10.1016/j.jhazmat.2020.122903.
[67] C.R. Kennedy, S. Lin, E.N. Jacobsen, The cation–π interaction in small-molecule, Catal. Angew. Chem. Int. Ed. 55 (2016) 12596–12624, https://doi.org/10.1002/anie.201600547.